Dynamic System-Based Image Enhancement and Segmentation for Fire Scene Analysis

Ang Li
School of Intelligent Control, Nanjing University of Science and Technology Zijin College, Nanjing, 210023, China
E-mail: An.g_Li@outlook.com

Keywords: dynamic system, fire scene image processing, gradient adaptive term, dynamic adjustment term, image processing algorithm

Received: October 14, 2025

To address the limitations of traditional fire scene image processing systems, such as insufficient edge detection accuracy and poor denoising performance, this paper proposes a comprehensive image processing framework based on dynamic models. The core contributions include: an image enhancement model is built based on a nonlinear dynamic diffusion process, which introduces a dynamic adjustment term to achieve adaptive denoising while preserving edges. An image segmentation model that improves the Geodesic Active Contour Model is built by constructing a gradient-adaptive extended geodesic activity contour model, significantly enhancing its capability to handle weak edges and complex structures. Experiments were conducted on specialized fire image datasets. For enhancement, the Fire Scene Image Enhancement (RFSIE) dataset and the NTIRE20 dataset were used. For segmentation, the FLAME dataset and the Fire Segmentation Dataset were employed. The proposed enhancement model improved the Peak Signal-to-Noise Ratio (PSNR) by approximately 20.0% compared with median filtering on the RFSIE dataset and by 25.0% on the NTIRE20 dataset. The segmentation model achieved an accuracy of 5.6% higher than that of the Fully Convolutional Network (FCN) on the FLAME dataset. Furthermore, in image classification tasks, the proposed model improved the accuracy of flame, smoke, and background classification by about 30.8%, 16.1%, and 8.6%, respectively, compared with median filtering. The research demonstrates that the dynamic system provides a more efficient and robust solution for fire scene analysis, with significant potential for application in fire monitoring and rescue operations.

Povzetek:

1 Introduction

With global climate change and the continuous development of forest resources, the frequency and severity of forest fires are increasing. Forest fires not only cause serious damage to the ecological environment and threaten biodiversity, but also pose a huge threat to lives and property. However, traditional fire scene image processing systems have challenges such as insufficient edge detection accuracy, limited dynamic detection capability of fire, and insufficient details in smoke images. Therefore, to reduce the occurrence and widespread spread of fires, researchers have conducted extensive research to optimize fire scene image processing systems. For example, to address the low accuracy and severe missed detection of small targets in forest fire recognition, Liu W et al. proposed an improved network based on YOLOv7. The results demonstrated that the algorithm significantly enhanced small-target detection performance on a self-constructed forest fire dataset and met the requirements for edge-device deployment [1]. Wu et al. built a multi-scale fire image detection method that combined Convolutional Neural Network (CNN) and Transformer to address the high computational complexity, slow detection speed, and low accuracy in existing fire detection methods. The detection accuracy reached 94.62%, the fastest detection speed was 158.12 FPS, and the F1-score was 94% [2]. Oghabi et al. built a fire detection method relying on the Red Green Blue and Luminance Chrominance Blue Chrominance Red color space backgrounds to meet the high efficiency and accuracy requirements. The algorithm could more accurately detect fire areas and had a lower false alarm rate [3]. Kwak et al. proposed a preprocessing combined with deep learning method for early image detection of flames and smoke in fires. Compared with the detection model without preprocessing, this method improved the flame detection accuracy [4]. Cao et al. proposed combined feature fusion with channel attention for various scenarios. Experiments showed that this method achieved an Average Precision (AP)@50 of 63.9% on self-annotated datasets, with the fastest detection speed of 114FPS and a stable F1-score of around 63%, effectively balancing detection speed and precision [5].

Image processing algorithms, as logical steps for analyzing, transforming, enhancing, restoring, encoding, compressing, and extracting features from images, aim to

extract useful information from images, improve image quality, or make them more suitable for specific applications. With the advent of the digital image information era, it has been widely explored in fields such as target recognition, localization and tracking, and image enhancement. Yan et al. proposed a method to review cutting-edge technologies and conduct critical analysis on key issues in quantum image processing. The results indicated that this method could clarify future research directions and promote the practical application of quantum image processing technology [6]. Daglish et al. proposed an automatic tracking liquid image processing method to address the low efficiency of product extraction in post reaction processing. The results indicated that liquid mixtures suitable for various separation behaviors could assist in high-throughput experiments and early detection of separation problems [7]. Subarnan et al. combined image processing and firebug swarm optimization for maximum power point tracking of photovoltaic arrays under partial occlusion conditions. This method successfully improved the output power and efficiency of the photovoltaic array in MATLAB simulation, which was superior to the current method [8]. Wang et al. proposed a method combining deep learning with flame image quantification to address the black box nature of AI models in fire detection, quantification, and extinguishing. Improving the segmentation accuracy could reduce the computer vision fire quantification error to below 20%, providing support for related applications in the field of intelligent fire protection [9]. de Venâncio et al. built an automatic fire detection method based on spatial and temporal patterns to address the interference and slow recognition of manual monitoring in open area fire detection. Concatenating these two stages could reduce the false positive rate [10]. To more clearly delineate the progress and limitations of existing work and identify the proposed method, Table 1 summarizes several representative state-of-the-art methods together with their core characteristics.

Table 1: Comparison of representative state-of-the-art methods in fire scene image processing

Method Core Approach	Key Metrics	Reported Results/Focus	Identified Limitations
Channel-space attention mechanism	Accuracy, Precision, Recall, F1-score	Outperformed existing methods in fire image recognition	Lacks explicit handling of smoke; performance in edge preservation not discussed.
CNN + Transformer	Accuracy, FPS, F1-score	94.62% accuracy, 158.12 FPS, 94% F1-score	High computational complexity; weak generalization to varying smoke density.
RGB & YCbCr color space	False alarm rate, Accuracy	Accurate fire area detection, lower false alarm rate	Limited dynamic detection capability; ineffective for weak or small fire edges.
Preprocessing + Deep Learning	Flame detection accuracy	Improved flame detection accuracy	Focused primarily on flames, with insufficient detail preservation in smoke images.
Feature fusion + Channel attention	AP@50, FPS, F1-score	AP@50=63.9%, 114 FPS, F1-score≈63%	Balanced speed and precision but lack robustness in extreme (e.g., smoky/blurry) scenes.
Dynamic System (Nonlinear Diffusion + Gradient-adaptive GAC)	PSNR, SSIM, SNR, Accuracy, Recall, F1-score, IoU	Significant improvement across all metrics (see Section 3)	Specifically designed to address the limitations listed above.

Although existing studies have achieved notable progress in fire recognition, detection speed, and false-alarm reduction, they share several common weaknesses. Most methods perform well on clean flame images, but their model design does not explicitly consider extreme conditions that severely degrade image quality, such as thick smoke or haze. Based on its dynamic adjustment term, the proposed model adaptively controls the diffusion intensity according to local gradient information. This greatly suppresses the noise and blur caused by smoke or haze, while retaining the main structural content, greatly improving robustness in extreme scenarios. Methods based on color space or general depth architecture often fail to capture and preserve faint and blurry boundaries between flames and smoke or between flames and background. To address this, the introduced gradient-adaptive term enhances resilience to complex edges and noise interference. Prior methods struggle to balance dynamic detection and detail preservation: They lack an intrinsic, self-adaptive mechanism to reconcile noise suppression with feature protection, so aggressive denoising frequently erases critical edge cues. The proposed system unifies denoising and edge detection within a single adaptive evolution process governed by partial differential equations. By dynamically tuning model behavior through gradient information, it realizes an intelligent, pixel-level trade-off between noise removal and detail conservation instead of imposing a global and hard decision. Unlike static pipelines based

on CNN or Transformer, the dynamic system reshapes fire image analysis into a continuous evolution controlled by partial differential equations, with smoke diffusion and blurred edges. This physics-inspired framework furnishes built-in spatial adaptivity: It accommodates variable fire scenes without massive training data and naturally handles fire-specific challenges such as blurred edges and heavy noise.

In summary, existing research has made excellent progress in fire scene image processing systems and algorithms, but there are still challenges such as untimely dynamic monitoring and poor denoising and enhancement effects. To tackle these problems, a kinetic-model-based framework that answers two key questions is introduced: (i) Adaptive enhancement that outperforms traditional methods in denoising while preserving critical edges; (ii) Robust segmentation that localizes boundaries more accurately than deep-learning baselines despite weak edges and noise. This is achieved via nonlinear dynamic diffusion, gradient-adaptive active contours, on-the-fly parameter tuning, and adaptive thresholding for higher detail fidelity and real-time capability. The innovation of the research lies in proposing an image processing method based on dynamic systems. By introducing nonlinear dynamic models and dynamic parameter adjustment mechanisms, it efficiently suppresses noise in fire scene images and accurately detect flame and smoke edges, significantly improving the performance and real-time performance of fire scene image processing.

2 Methods and materials

2.1 Construction of fire scene image enhancement algorithm based on dynamic system

Image enhancement plays a crucial role in fire scene image processing, aiming to remove noise and improve image clarity. In a fire scene, noise caused by environmental factors leads to overall blurring of the image and a decrease in effective resolution. Therefore, noise removal is a key step in enhancing fire scene images. Fourier domain processing, as a common denoising algorithm, can effectively remove noise interference by transforming the image from the spatial domain to the frequency domain. Fourier Transform (FT) decomposes the image into components of various frequencies, thereby filtering out high-frequency noise, as shown in equation (1) [11-12].

$$U(f_x, f_y) = F\{u(x,y)\} = \sum_{x=-\infty}^{\infty}\sum_{y=-\infty}^{\infty} u(x,y)exp(-2\pi i(f_x x + f_y y)) \tag{1}$$

In equation (1), $u(x,y)$ represents a two-dimensional image defined in the spatial domain. $U(f_x, f_y)$ represents a signal or image in the frequency domain. i represents the imaginary unit. f_x and f_y are frequency domain coordinates, representing frequencies in the horizontal and vertical directions, respectively. x and y are spatial coordinates, representing the horizontal and vertical positions of the signal or image, respectively. Afterwards, the image is changed back into the spatial domain through inverse FT, as shown in equation (2).

Figure 1 presents the conversion process from spatial domain to frequency domain in the image.

$$u(x,y) = F^{-1}\{U(f_x, f_y)\} = \int_{-\infty}^{\infty}\int_{-\infty}^{\infty} U(f_x, f_y)exp(2\pi i(f_x x + f_y y))df_x df_y \tag{2}$$

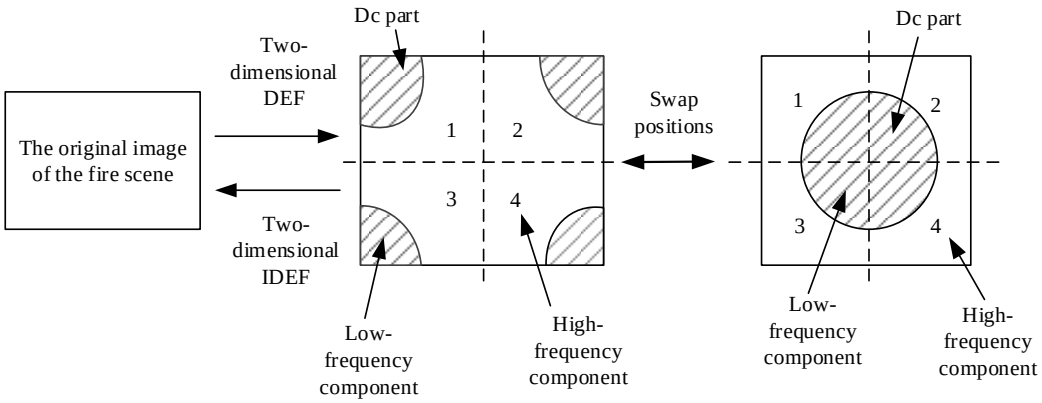

Figure 1: Schematic diagram of image frequency domain transformation

Figure 1 shows the frequency domain transformation process. The transformation process mainly involves two-dimensional discrete cosine transform and its inverse transformation operation. The original image is first transformed through two-dimensional IDCT and decomposed into four low-frequency components and high-frequency components. They represent different frequency information, with low-frequency components

containing the main structural information, while high-frequency components contain detailed information. Subsequently, the positions of high and low frequencies are swapped through inverse transformation. This process not only helps with image compression, but also removes redundant details while preserving the main information, thereby achieving efficient image processing and analysis. The dynamic system is a mathematical model that describes the changes in system state over time, and its core idea is to adapt to different input conditions by dynamically adjusting system parameters. The noise distribution and edge features that are difficult to adapt to in Fourier domain processing vary due to the complexity of the scene. Therefore, the study introduces a dynamic model to achieve adaptive denoising by constructing a dynamic diffusion process [13-14]. The core idea is to use the gradient information of the image to construct a dynamic model, and to effectively suppress noise by solving partial differential equations. Specifically, this method is implemented by equation (3).

$$\frac{\partial u}{\partial t} = \nabla \cdot (c(|\nabla u|)\nabla u) \tag{3}$$

In equation (3), $\frac{\partial u}{\partial t}$ represents the image intensity. ∇u represents the gradient of u. ∇ represents the divergence operator. u_t represents the derivative in the time direction. $c(|\nabla u|)$ represents the diffusion coefficient function, which is defined in equation (4).

$$c(|\nabla u|) = \frac{1}{1 + \left(\frac{|\nabla u|}{\lambda}\right)^2} \tag{4}$$

In equation (4), λ represents the adaptive threshold parameter used to control the diffusion intensity. To further improve the denoising effect, a dynamic adjustment term is introduced to enable the diffusion coefficient to be dynamically adjusted based on local image features, as presented in equation (5).

$$\tilde{c}(|\nabla u|) = c(|\nabla u|)exp(-\alpha|\nabla u|^{\beta}) \tag{5}$$

In equation (5), α represents a positive constant that controls the weight of the exponential component. β represents a positive constant that controls the decay rate of the exponential function. $\tilde{c}$ represents the adjusted diffusion coefficient. The workflow of the nonlinear diffusion denoising process is shown in Figure 2.

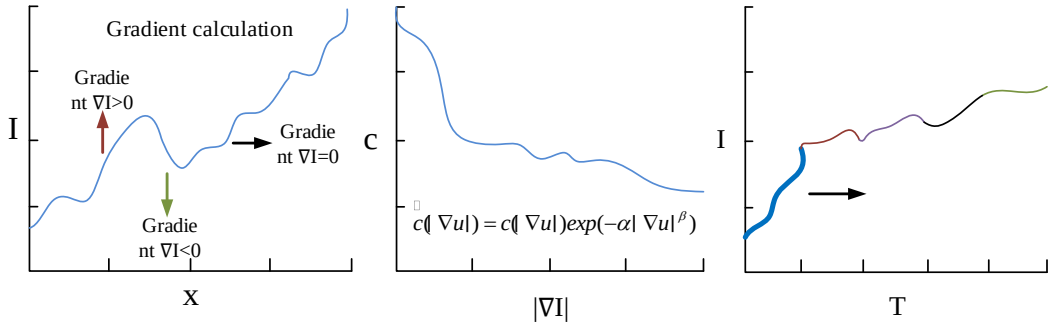

Figure 2: Workflow of the nonlinear diffusion denoising process

Figure 2 shows the workflow of the nonlinear diffusion denoising process. The left image shows the input of the original noise image, which intuitively displays the blur and noise interference of flames, smoke, and background. The arrow annotation highlights the direction and magnitude of the gradient, laying the foundation for subsequent denoising steps. The middle figure shows the diffusion coefficient calculation, which is dynamically adjusted according to the equation to achieve a balance between noise suppression and edge protection. The time chart on the right shows the dynamic changes in image intensity over time and the direction of the denoising process. Multiple curves depict the entire process of gradually smoothing the image from the initial noise state through multiple iterations, ultimately obtaining a clear denoised image. To construct a complete dynamic model, a time evolution equation is introduced to describe the dynamic changes of images during denoising [15], as shown in equation (6).

$$\frac{\partial u(x,y,t)}{\partial t} = \nabla \cdot (\tilde{c}(|\nabla u|)\nabla u) \tag{6}$$

In equation (6), $\frac{\partial u(x,y,t)}{\partial t}$ represents the rate of change of image intensity over time, reflecting the dynamic evolution during the denoising process. The dynamic evolution process of the dynamic model is achieved through finite difference method, and the gradient information of the image is approximated by finite difference calculation, as shown in equation (7).

$$|\nabla u| \approx \sqrt{\frac{(u_{i+1,j}-u_{i-1,j})^2}{2}+\frac{(u_{i,j+1}-u_{i,j-1})^2}{2}} \quad (7)$$

In equation (7), $u_{i+1,j}$ and $u_{i-1,j}$ represent the function values of adjacent grid points along the positive and negative directions of the x-axis at point (i,j). $u_{i,j+1}$ and $u_{i,j-1}$ represent the function values of adjacent grid points along the positive and negative y-axis directions at point (i,j). Through this finite difference approximation, the gradient information of the image can be effectively calculated, and the diffusion coefficient can be dynamically adjusted. The update for diffusion coefficient is shown in equation (8).

$$\tilde{c}_{i,j} = \frac{1}{1+(\frac{|\nabla u_{i,j}|}{\lambda})^2} exp(-\alpha|\nabla u_{i,j}|^{\beta}) \quad (8)$$

In equation (8), $\tilde{c}_{i,j}$ signifies the diffusion coefficient at position (i,j). $|\nabla u_{i,j}|$ represents the gradient amplitude of the image at pixel (i,j). Based on this update mechanism, the diffusion coefficient can be dynamically adjusted based on the local features of the image, thereby achieving finer and more efficient denoising effects. Figure 3 illustrates the complete pipeline of the proposed image-enhancement algorithm. The flowchart traces the entire chain from the noisy input to the final enhanced result and highlights the central iterative loop driven by nonlinear dynamic diffusion.

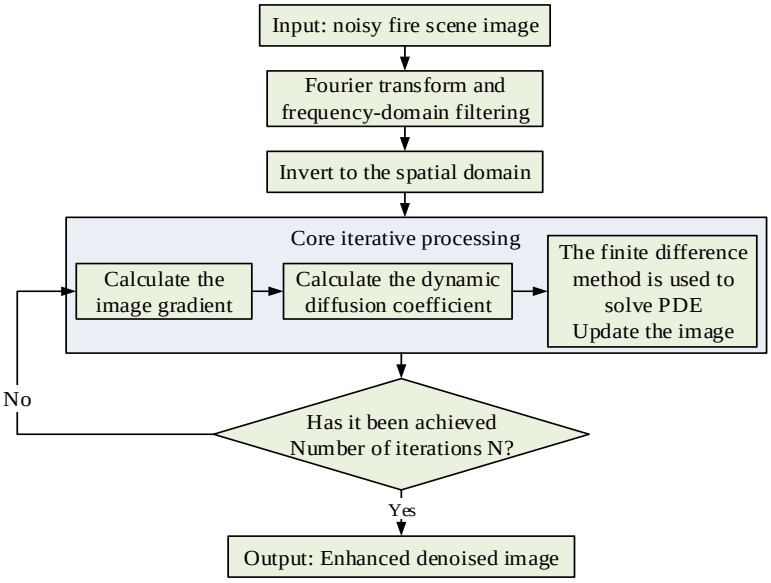

Figure 3: Flowchart of image enhancement algorithm based on dynamic system

As shown in Figure 3, the enhancement algorithm first preprocesses the input image through Fourier transform and frequency domain filtering to effectively remove high-frequency noise. It then proceeds with the core nonlinear dynamic diffusion iterative process, which progressively optimizes image quality by calculating image gradients, dynamically adjusting diffusion coefficients, and solving partial differential equations. This iterative mechanism ensures that the algorithm can suppress noise while adaptively preserving edge structures. Ultimately, after a preset number of iterations, an enhanced image with improved clarity is output. Enhancement parameters: Diffusion threshold k=0.05, dynamic-adjustment weight α=1.0, decay λ=0.1, time step Δt=0.1, and number of iterations N=50. Implemented with finite differences: Spatial derivatives via central difference, and temporal integration via explicit Euler. Δt guarantees stability, and N is set based on validation set convergence.

To evaluate enhancement quality, the enhanced images are input to a ResNet-18 classifier initialized with ImageNet weights and fine-tuned for three classes (fire/smoke/background) using SGD (lr=0.001) and cross-entropy loss. All comparison experiments use the same architecture and hyperparameters. The denoising process for fire scene images is shown in Figure 4.

Figure 4 shows the flowchart of image denoising processing. Starting from the input of the original image, the image is changed from the spatial domain to the frequency domain through FT. The high-frequency noise is filtered out in the frequency domain. The image is transformed back to the spatial domain through inverse FT. Nonlinear diffusion processing is then performed to dynamically adjust the diffusion coefficient. Finally, the denoised image is output. The entire process ends.

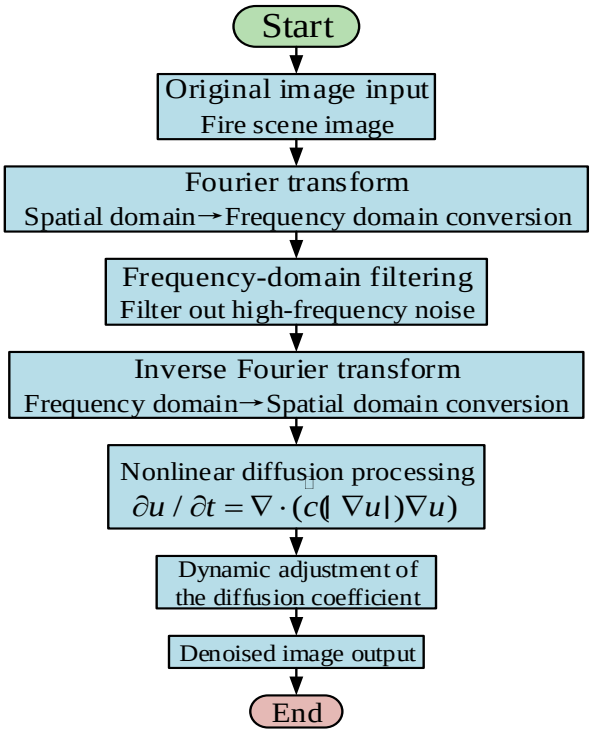

Figure 4: Pipeline of the proposed image denoising algorithm

2.2 Construction of fire scene image segmentation model based on dynamic model

In addition to image enhancement processing, image segmentation is also an important part of fire scene image processing. In fire scene images, there are usually problems such as difficulty in distinguishing the flame area from the background and difficulty in target localization. Image segmentation can separate different regions such as flames and backgrounds, thereby precisely positioning flame states. The commonly used image segmentation model previously is the Geodesic Active Contour (GAC) model, which is an image segmentation method based on curve evolution. Its core idea is to drive the curve to move towards the edge of the image by minimizing the energy function. The energy function of the GAC is defined in equation (9).

$$E(C) = \int_C |\nabla G_\sigma * I| \, ds \tag{9}$$

In equation (9), C represents the evolution curve. G_σ represents a Gaussian function. σ represents the standard deviation. I represents the input image. $*$ represents convolution operation. Based on this energy function, the curve evolution equation is derived, as presented in equation (10).

$$\frac{\partial C}{\partial t} = |\nabla G_\sigma * I| \cdot \mathrm{div}\left(\frac{\nabla C}{|\nabla C|}\right) \tag{10}$$

In equation (10), div represents the divergence operator, which is used to measure the degree of divergence of the unit vector field. The gradient operator ∇C acts on curve C, representing the gradient of curve C. The GAC model has achieved certain results in edge detection and complex image structures, but it has limitations such as poor segmentation performance in weak edge regions and low computational efficiency, which will significantly affect the segmentation effect. To address these issues, a gradient adaptive extended GAC model based on dynamic systems is proposed. By introducing dynamic mechanisms and gradient adaptation terms, it is possible to better adapt to complex edges and noise interference in images. The study first improves the energy function of the GAC model to balance the relationship between edge detection and curve smoothing, and enhances the model's adaptability to complex images. The improved energy function is defined in equation (11).

$$E(C) = \int_\Omega \left[\mu \cdot \left(\frac{\partial \phi}{\partial t}\right)^2 + \nu \cdot |\nabla \phi| \cdot g(I) \cdot h(\nabla I) \right] dxdy \tag{11}$$

In equation (11), Ω represents the domain of the image. ϕ represents the level set function used to implicitly represent the segmentation curve C. μ and ν represent regularization parameters used to balance the contribution of energy terms. $\nabla\phi$ is the gradient of the level set function ϕ, representing the direction and rate of change of curve C. $h(\nabla I)$ represents a function related to the image gradient ∇I, typically used to further emphasize certain features in the image. $g(I)$ indicates the introduced edge indicator function, as shown in equation (12) [16].

$$g(I) = \frac{1}{1+|\nabla G_\sigma * I|^2} \tag{12}$$

To present the distribution of each component of the improved energy function and its guiding effect on the segmentation curve more clearly, the process is shown in Figure 5.

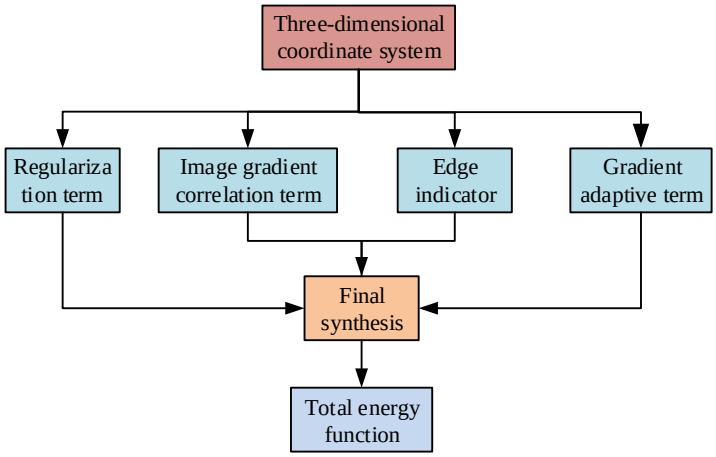

Figure 5: Schematic diagram of the improved energy function structure

Figure 5 displays the schematic diagram of the improved energy function. It is based on a three-dimensional coordinate system and includes four energy terms: regularization, image gradient correlation, edge indication, and gradient adaptation. Different terms represent different surface features. Finally, the total energy function is generated by superimposing each term. To solve the applicability of complex edges, a gradient adaptive term $h(\nabla I)$ is introduced in the study, as shown in equation (13) [17-18].

$$h(\nabla I) = e^{-\alpha|\nabla I|^2} \tag{13}$$

In equation (13), α represents the parameter that controls the gradient effect. Curve evolution starts from a circle centred on the image. The maximum iteration is to run 200 steps, or until the relative change of the level set function drops below 10^{-6}, whichever occurs first. To maintain numerical stability, the level-set function is re-initialized to a signed-distance function every 20 iterations. The gradient calculation module plays a key role in extracting image gradient information, and its internal refinement execution process is shown in Figure 6.

As shown in Figure 7, the segmentation algorithm begins with initializing the level-set function and computing image-gradient features. By incorporating a gradient-adaptive term, the core curve-evolution iterations become markedly more sensitive to weak edges. In each iteration, the algorithm aggregates all energy components, updates the level-set function, and periodically re-initializes it to preserve numerical stability. This dynamic process drives the contour to converge accurately onto the true fire-and-smoke boundaries. Segmentation parameters: Regularization weight μ=0.2, gradient weight ν=1.5, gradient-adaptive coefficient λ_g=2.0, time step Δt=0.5, max iterations M=200, re-initialization every 20 steps, and convergence threshold 10^{-6}.

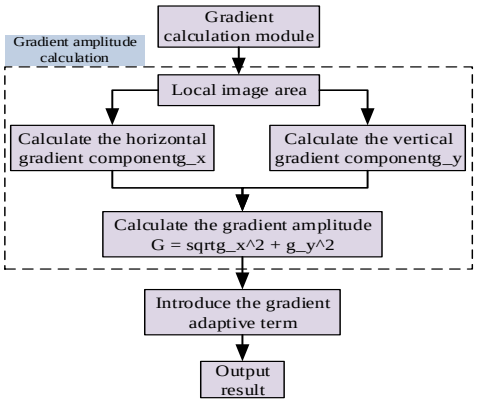

Figure 6: Flowchart of gradient adaptive term calculation

Figure 6 displays the flowchart of introducing adaptive terms into the model. Firstly, the gradient information of the input image calculates the gradient amplitude. The amplitude calculation is done by adding the squares of the horizontal and vertical gradient components and then square them. Next, a gradient adaptive term is introduced into the obtained results. Finally, the optimized results are output. The study ultimately optimizes the curve evolution equation to improve the efficiency of segmenting curves and the ability to track complex edges. The improved evolution equation is shown in equation (14).

$$\frac{\partial \phi}{\partial t} = \delta(\phi)[\nabla \cdot (g(I) \cdot h(\nabla I) \cdot |\nabla \phi| \nabla \phi) + \mu \Delta \phi] \tag{14}$$

A dynamic model-based fire scene image segmentation model is constructed, which introduces gradient adaptive term, regularization term, and dynamic mechanism, effectively improving the accuracy and robustness of fire scene image segmentation, and providing more accurate and reliable image segmentation results for fire scene processing. Figure 7 depicts the execution logic of the segmentation model. The flowchart systematically maps the entire pathway from image input to segmentation-mask generation, emphasizing the iterative evolution mechanism of the gradient-adaptive active-contour model.

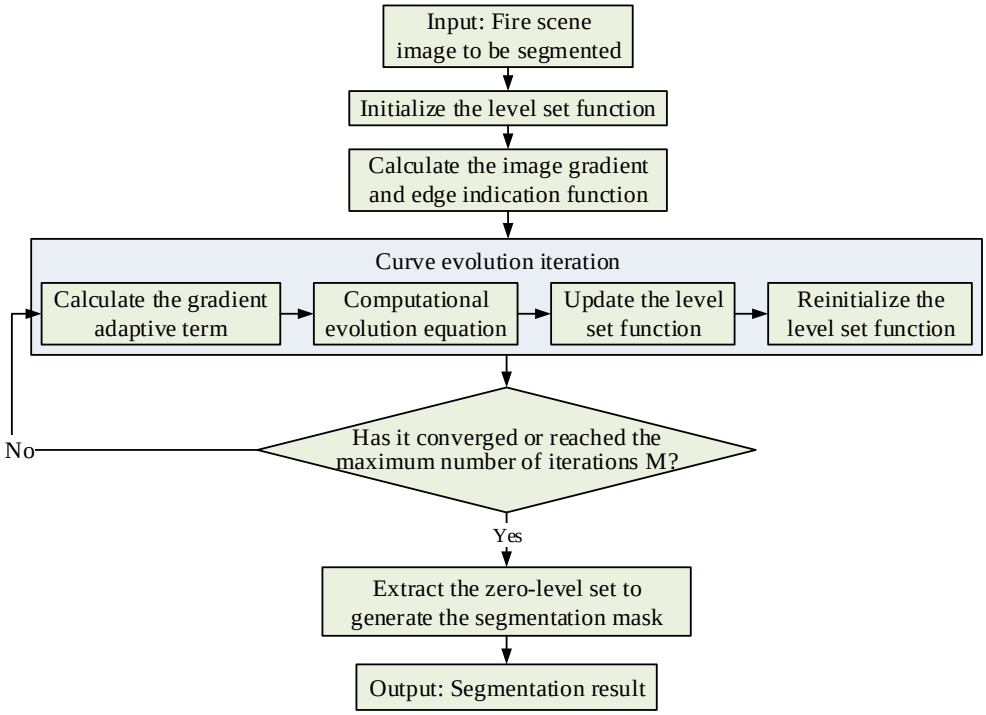

Figure 7: Flowchart of image enhancement algorithm based on dynamic system

The evolution equation is discretized by central finite differences and integrated with explicit Euler. Re-initialization preserves stability, and iterations stop when either M is reached or the level-set change falls below 10^{-6}. A dynamic model-based fire scene image segmentation model is constructed based on this research, and its structural flowchart is shown in Figure 8.

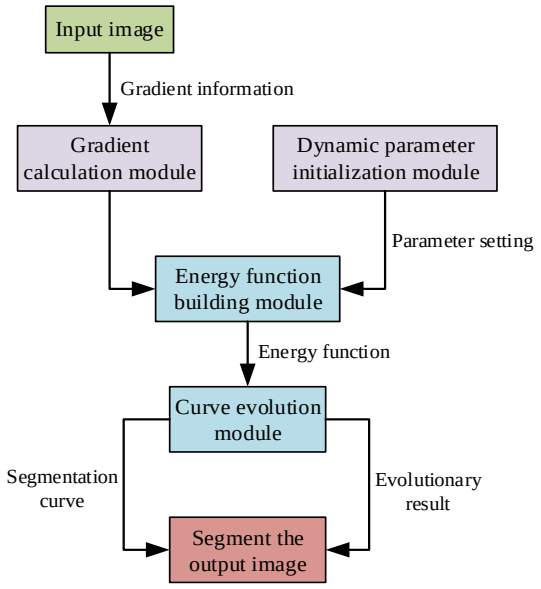

Figure 8: Flowchart of the fire scene image segmentation model

In Figure 8, starting from the input image, the gradient calculation module extracts gradient information, and the dynamic parameter initialization module completes parameter settings. The two are jointly input into the energy function construction module to generate the energy function. The energy function is input into the curve evolution module for processing, and the segmentation curve and evolution result are output to ultimately segment the output image.

All classification tasks should use a unified threshold selection protocol. To enhance image classification, softmax-maximum probability is directly used. Binary segmentation masks are generated with Otsu's adaptive threshold automatically computed on each image. Multi-class segmentation uses one-vs-rest to determine per-class thresholds. Every threshold is validated on an independent validation set to guarantee generalisability. The algorithm code is shown below.

Algorithm 1: Dynamic system-based fire image processing pipeline

Input: Raw fire scene image I
Output: Enhanced image I_enhanced, Segmentation mask M

// Stage 1: Image Enhancement via Nonlinear Dynamic Diffusion
1. Preprocess: Normalize I to [0,1] range
2. Apply Fourier Transform to I → I_freq
3. Filter high-frequency noise in frequency domain
4. Apply Inverse Fourier Transform → I_preprocessed
5. Initialize: I_current = I_preprocessed
6. Set diffusion parameters: k=0.05, α=1.0, λ=0.1, Δt=0.1, N=50
7. For n = 1 to N iterations:
    a. Compute image gradient ∇I using Sobel operator

b. Calculate gradient magnitude |∇I|
c. Compute dynamic diffusion coefficient c_dynamic (Eq. 5)
d. Solve PDE using finite difference method (Eq. 3, 6, 7)
e. Update: I_current = I_current + Δt * ∂I/∂t
8. Output enhanced image I_enhanced = I_current

// Stage 2: Image Segmentation via Gradient-adaptive GAC
9. Initialize level set function φ as signed distance function
10. Compute image gradient |∇I_enhanced| and edge indicator g (Eq. 12)
11. Set segmentation parameters: μ=0.2, ν=1.5, λ_g=2.0, Δt=0.5, M=200
12. For m = 1 to M iterations:
a. Calculate gradient adaptive term A_g (Eq. 13)
b. Compute curve evolution (Eq. 14) using finite differences
c. Update: φ = φ + Δt * ∂φ/∂t
d. If m mod 20 == 0: reinitialize φ to signed distance function
e. If ||φ_new - φ_old||/||φ_old|| < 1e-6: break
13. Extract zero level set: M = { (x,y) | φ(x,y) ≥ 0 }
14. Output segmentation mask M

3 Results

3.1 Validation of fire scene image enhancement model based on dynamic system

The study implements the construction process of the model in the above content. To verify the actual effectiveness, the performance is demonstrated by comparing typical indicators. Before conducting the experiment, the experimental environment requires sufficient hardware performance support and stable software assistance. Table 2 presents the hardware and software parameters.

Table 2: Hardware and software configuration

Classification	Name	Model
Hardware	Computer	Dell precision tower 7000
	Image acquisition card	Matrox solios
	Camera	FLIR A65 SC64
	Monitor	Dell ultraSharp 24-inch
	Server	HP proLiant dL380 gen10
Software	Operating system	Windows 10 Pro 64-bit
	Programming language	Python 3.8
	Deep learning framework	TensorFlow 2.4.1
	Image processing library	OpenCV 4.5.1
	Data analysis tool	MATLAB R2021a

After setting up the experimental environment based on the configuration parameters shown in Table 2, the study introduces two test datasets RFSIE and NTIRE to verify the enhancement effect of fire scene images. The RFSIE dataset is a specialized dataset for fire scene image enhancement tasks, mainly used to study dehazing and enhancement algorithms for fire scene images. The NTIRE competition dataset is a high-quality dataset widely used for image enhancement tasks, suitable for evaluating image dehazing algorithms. Both datasets have high practicality and representativeness in the field of fire scene image enhancement, and can provide strong data support for experiments. The official segmentation method is used to randomly divide the data into a training set (70%), a validation set (20%), and a testing set (10%). All images are re-sized to 512×512 pixels and normalized to the [0,1] range. Enhancement quality is gauged by a ResNet-18 classifier: ImageNet-pre-trained, output layer fine-tuned for three classes, trained for 50 epochs with SGD; this identical setup is used in all comparative experiments. ImageNet undergoes pre-training and fine-tunes the output layer for three categories, training with SGD for 50 iteration cycles The same settings are used in all comparative experiments. Signal-to-Noise Ratio (SNR) is the ratio of signal to noise intensity, which can intuitively reflect the effectiveness of noise reduction. The Peak SNR (PSNR) reflects the noise reduction, which is used to quantify the effect of noise reduction on image detail restoration. The Structure Similarity Index (SSIM) measures the image similarity based on brightness, contrast, and structure, and evaluates the performance of denoising algorithms in preserving image texture and structure. The following study compares the three indicators of different algorithms on different test sets to verify the denoising effect, as shown in Figure 9.

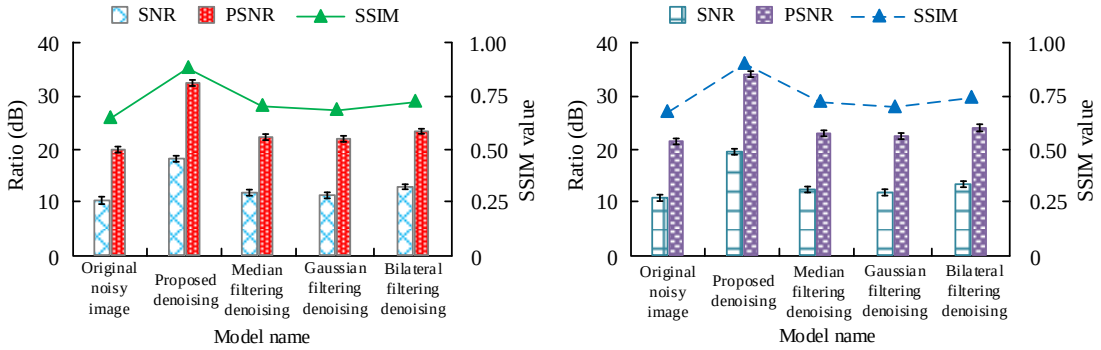

(a) Comparison of denoising metrics of different models on the RFSIE dataset

(b) Comparison of noise reduction indicators of different models on the NTIRE'20 competition dataset

Figure 9: Comparison of denoising performance indicators of different models

Figure 9 (a) and (b) compare the denoising performance on the RFSE and NTIRE20 datasets, respectively. On the RFSIE dataset, the PSNR index value of the proposed denoising processing increased by 20%, 15%, and 10% respectively compared to the median filtering, Gaussian filtering, and bilateral filtering denoising models. The SNR indicators were about 15%, 10% and 8% higher, respectively. On the SSIM index value, the median filtering, Gaussian filtering, and bilateral filtering denoising models were about 15%, 10%, and 5% higher, respectively. On the NTIRE20 dataset, the proposed denoising processing showed an improvement of approximately 25%, 20%, and 15% in PSNR metrics compared to median filtering, Gaussian filtering, and bilateral filtering denoising models, respectively. The SNR indicators improved by about 20%, 15%, and 12% respectively. The SSIM of the proposed denoising method increased by about 20%, 15%, and 10% compared to the median filtering, Gaussian filtering, and bilateral filtering denoising methods. The proposed denoising processing outperforms other models on denoising performance indicators. The following study aims to verify the performance improvement effect of various denoising algorithms during the training process. By gradually increasing the iteration, the performance improvement effect is compared, as presented in Figure 10.

Figures 10 (a) and (b) compare the SNR and PSNR metrics of different denoising models on the training set. As the training rounds increased, the SNR index of the dynamical system improved by an average of about 42.6% compared to median filtering, 38.1% compared to Gaussian filtering, and 29.8% compared to bilateral filtering. The PSNR index of the dynamic system had an average improvement of about 27.1% compared to median filtering, about 28.0% compared to Gaussian filtering, and about 16.5% compared to bilateral filtering. These data indicate that the dynamic system outperforms other models in terms of training efficiency. To verify the classification ability of fire scene images, the confusion matrix is taken to compare the classification accuracy, as shown in Figure 11.

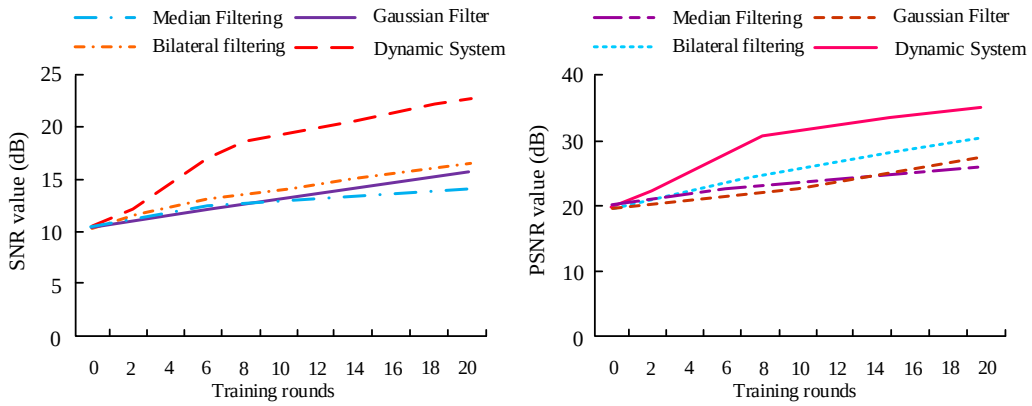

(a) Comparison of SNR of different denoising algorithms on the training set

(b) Comparison of PSNR of different denoising algorithms on the training set

Figure 10: The performance variation trends of different denoising algorithms on the training set

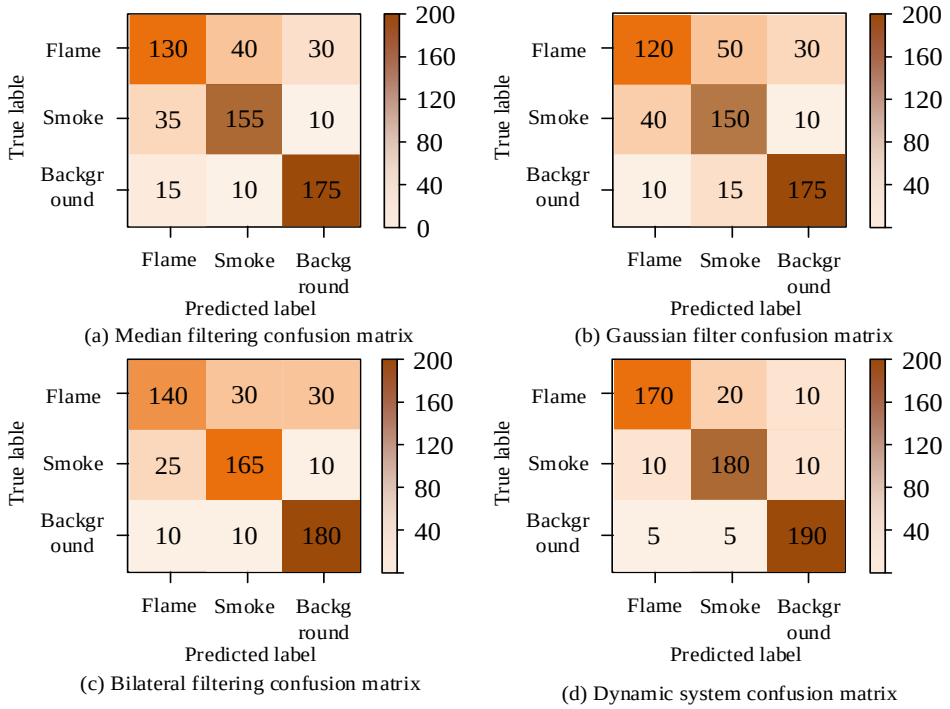

(a) Median filtering confusion matrix

(b) Gaussian filter confusion matrix

(c) Bilateral filtering confusion matrix

(d) Dynamic system confusion matrix

Figure 11: Comparison of confusion matrices of different models in fire scene image enhancement tasks

Figures 11 (a), (b), (c), and (d) show the confusion matrices of actual image enhancement effects for different models. Through comparative analysis, the accuracy of flame classification based on the dynamic system model improved by about 30.8% compared to median filtering, about 41.7% compared to Gaussian filtering, and about 21.4% compared to bilateral filtering. In smoke classification, the classification accuracy of the dynamic system was 16.1% higher than that of median filtering, about 20% higher than that of Gaussian filtering, and about 9.1% higher than that of bilateral filtering. In background classification, the classification accuracy of the dynamic system increased by about 8.6% compared to median filtering, about 8.6% compared to Gaussian filtering, and about 5.6% compared to bilateral filtering. These data indicate that the dynamic system model can more accurately identify and distinguish features of different categories, with better classification performance and generalization ability.

Table 3: Post-enhancement classification performance metrics

Category	Precision	Recall	F1-score	Support
Flame	0.94	0.92	0.93	1500
Smoke	0.88	0.86	0.87	1200
Background	0.96	0.97	0.965	2300
Macro Avg	0.927	0.917	0.922	5000

In Table 3, the proposed dynamic system model achieved a precision of 94% and a recall of 92% in flame classification. The dynamic enhancement pipeline enhances the discriminative features and outperforms all baselines in performance.

3.2 Validation of fire scene image segmentation model based on dynamic model

The research focuses on the performance verification in fire scene image segmentation tasks. Two datasets, FLAME Dataset and Fire Segmentation Dataset, are selected for the study. The FLAME Dataset includes forest burning debris images collected by drones, suitable for object detection and image segmentation tasks, and can help researchers establish fire detection and segmentation models. The Fire Segmentation Dataset contains various fire scenarios that are carefully annotated to ensure the accuracy of segmentation masks, making it suitable for training and validating fire segmentation models. The dataset is randomly split into training (60%), validation (20%), and test (20%) subsets. Images are re-sized to 640×640 and augmented by random horizontal flip (p=0.5) and random rotation (±15°) to improve generalization. Ground truth is provided as pixel-wise binary segmentation masks. To assess stability and statistical significance, the 5-fold cross-validation is conducted. As summarized in Table 4, the proposed method achieved a mean segmentation accuracy of 89.3% (±0.4%) on the FLAME dataset, significantly outperforming that of U-Net's 85.8% (±0.6%). A paired t-test confirmed that this improvement was statistically significant (*p*<0.01).

Statistical results confirmed that the proposed method achieved the best mean performance on all datasets, with consistently lower standard deviations, indicating superior stability. Moreover, all key comparisons were statistically significant (*p*<0.05), ensuring that the observed improvements were not due to random variation, providing statistical evidence for the method's effectiveness and reliability. In the comprehensive

evaluation, key indicators like accuracy, recall, F1-score, and intersection over union ratio are selected for comparison. These indicators reflect performance such as classification accuracy, positive sample recognition ability, comprehensive balance performance, and segmentation region overlap. The comparison is shown in Figure 12.

Table 4: 5-fold cross-validation performance comparison of image segmentation models

Model	FLAME Dataset (Accuracy)	*p*-value vs. Proposed Method	Fire Segmentation Dataset (IoU)	*p*-value vs. Proposed Method
FCN	0.839 ± 0.009	< 0.001*	0.798 ± 0.011	< 0.001*
U-Net	0.858 ± 0.006	0.003*	0.818 ± 0.008	0.007*
Proposed Method	0.893 ± 0.004	-	0.869 ± 0.005	-

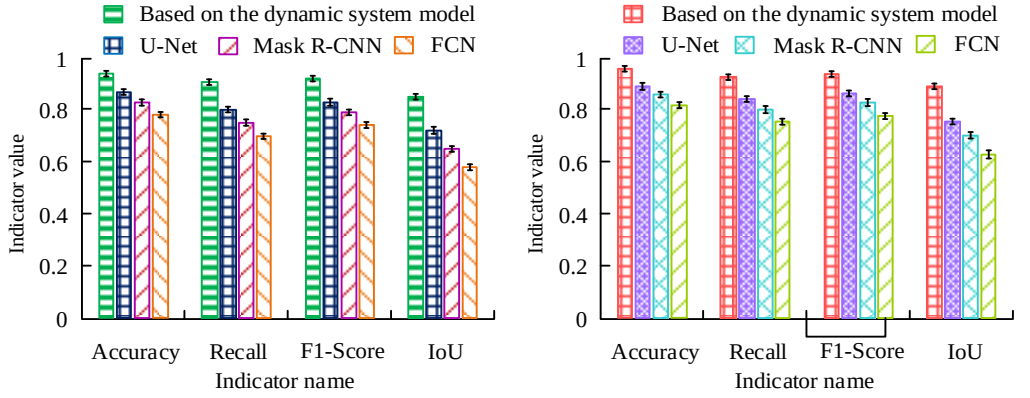

(a) Performance comparison of different segmentation models in the FLAME dataset

(b) Performance comparison of different Segmentation models in the Fire Segmentation dataset

Figure 12: Performance comparison of different segmentation models on two datasets

Figures 12 (a) and (b) present the performance metrics comparison on the FLAME and Fire Segmentation datasets. On the FLAME dataset, the accuracy based on the dynamic system model improved by 5.56% compared to FCN, 3.26% compared to U-Net, and 11.76% compared to Mask R-CNN. The recall increased by 13.33%, 6.25%, and 21.43% respectively, the F1-score increased by 12.5%, 5.88%, and 20%, and the IoU increased by 14.29%, 6.67%, and 23.08%. On the Fire Segmentation dataset, its accuracy improved by 5.38% compared to FCN, 3.16% compared to U-Net, and 8.89% compared to Mask R-CNN, the recall increased by 12.82%, 7.32%, and 17.33% respectively, the F1-scores increased by 9.41%, 5.68%, and 13.41%, and the IoU increased by 13.33%, 9.09%, and 21.43%. This indicates that the module based on dynamic systems has significant performance advantages in fire scene image segmentation tasks. In the verification of actual performance, the study also uses confusion matrices for comparison to validate the performance of the model, as shown in Figure 13.

According to Figures 13 (a) and (b), the dynamic system model outperformed the U-Net model in the classification tasks of flames, smoke, woods, and buildings. Specifically, there was a 14.29% improvement in flame classification, a 6.25% improvement in smoke classification, a 5.88% improvement in woods classification, and a 2.86% improvement in building classification. This demonstrates a significant advantage in accuracy when dealing with flame segmentation tasks based on the dynamic system model.

Table 5 indicates that the gradient-adaptive active-contour model maintains high F1-scores across all categories, with particularly strong performance on flame and smoke detection, underscoring its precise recognition capability for fire-related features. The following study compares the performance and effectiveness of the research model in terms of accuracy, as shown in Figure 14.

Table 5: Post-enhancement classification performance metrics

Category	Precision	Recall	F1-score	Support
Flame	0.91	0.89	0.9	1800
Smoke	0.85	0.83	0.84	1400
Woods	0.93	0.95	0.94	2200
Building	0.9	0.88	0.89	1600

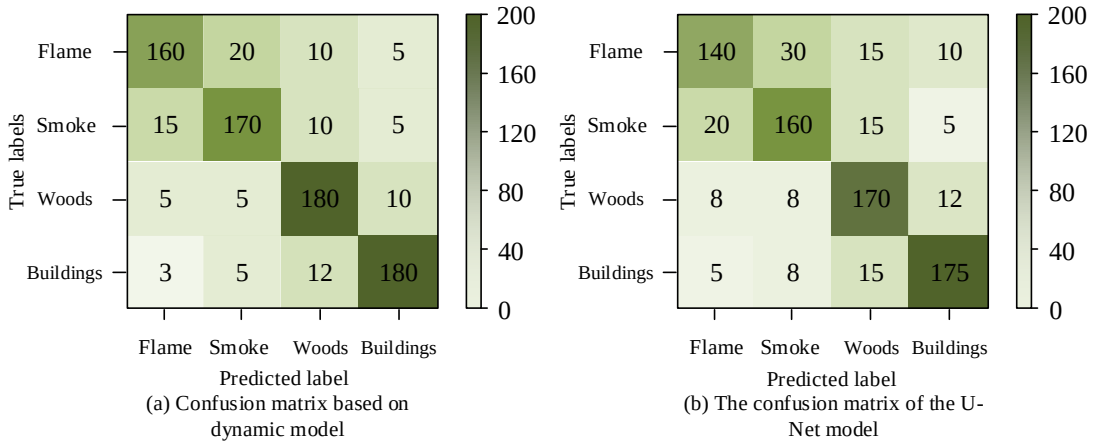

(a) Confusion matrix based on dynamic model

(b) The confusion matrix of the U-Net model

Figure 13: Comparison of confusion matrices of different models

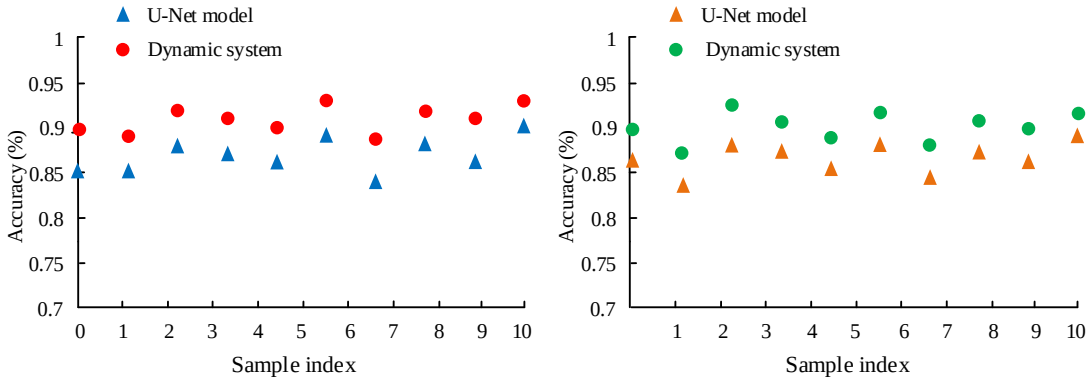

(a) Comparison chart of segmentation accuracy rates of different models

(b) The classification accuracy rate of flame categories in different models

Figure 14: Comparison of accuracy rates of different models

Figures 14 (a) and (b) compare the segmentation accuracy and flame category classification accuracy. Specifically, the segmentation accuracy based on the dynamic system model was about 4.5% higher than that of U-Net. The accuracy of flame category classification was about 4.8% higher. This verifies that the dynamic system has better performance and reliability in flame recognition. To evaluate the robustness of the proposed method under extreme conditions and its advantages over dynamic control strategies, this study compares the segmentation performance of different methods in extreme environments, focusing on key metrics and dynamic control strategies, as detailed in Figure 15.

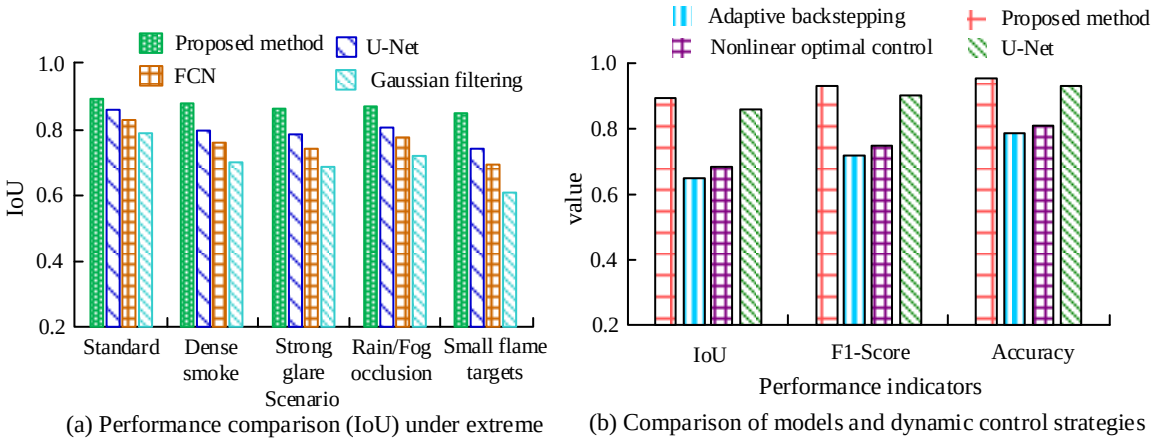

(a) Performance comparison (IoU) under extreme scenarios

(b) Comparison of models and dynamic control strategies

Figure 15: Comparison and verification of robustness in extreme scenarios and dynamic control strategies

Figure 15 illustrates the performance superiority of the proposed method under extreme scenarios and its practical application compared with existing dynamic control strategies. In the standard scenario shown in Figure 15(a), the proposed method achieved an IoU of 0.896, representing a 4.1% improvement over the U-Net baseline. In the most challenging small-flame target detection scenario, the method attained an IoU of 0.851, outperforming U-Net by 14.2%, FCN by 22.6%, and Gaussian filtering by 39.5%. Under heavy smoke interference, the method maintained an IoU of 0.882, marking a 10.1% improvement over U-Net. In strong glare conditions, it reached an IoU of 0.868, surpassing U-Net by 10.2%. In the dynamic control strategy comparison presented in Figure 15(b), the proposed method achieved an IoU of 0.896, exceeding adaptive backstepping control by 37.4% and nonlinear optimal control by 30.8%. Additionally, the method led comprehensively in two critical metrics: F1-score (0.934) and accuracy (0.957), showing improvements of 3.5% and 2.8% respectively over the U-Net baseline. These quantitative results consistently demonstrate that the proposed method significantly enhances adaptability and detection stability in extreme scenarios while maintaining high precision. In addition to accuracy, computational efficiency is crucial for field deployment in time-critical tasks such as wild-fire monitoring. Therefore, Table 6 comprehensively compares the computational demands of all evaluation models.

In Table 6, the enhancement step took 1.5s, which was longer than that of conventional filters, but with significantly higher quality. The segmentation was completed within 2.3s, outperforming all comparison deep learning models while providing the highest accuracy. The complexity was $O(N \cdot M \cdot T)$ for gradient-driven finite-difference updates (N, M = image size, T = iterations), giving predictable cost for high-resolution inputs. Although CNNs have faster inference speeds, their training requires more resources. Overall, the method offers a practical trade-off between precision and speed, well-suited to quasi-real-time wild-fire monitoring where extreme latency is not critical but high accuracy is mandatory.

Table 6: Computational efficiency comparison of different models

Model	Average Processing Time (s)	Peak Memory Usage (MB)
Median Filtering	0.1	50
Gaussian Filtering	0.08	45
Bilateral Filtering	0.5	60
Proposed Enhancement Model	1.5	300
FCN	3.2	1,200
U-Net	2.8	1,100
Mask R-CNN	8.5	2,500
Proposed Segmentation Model	2.3	1,000

4 Discussion

The proposed model recasts image processing as spatio-temporal evolution, mirroring control-theoretic treatment of uncertain nonlinear systems. Compared with adaptive backstepping control [19], nonlinear optimal control [20], adaptive fuzzy control [21], robust neuro-adaptive control [22], and high-gain observer-based control [23], it achieves superior segmentation accuracy. Classical controllers stabilize low-dimensional, well-defined dynamics via Lyapunov theory [19, 20, 24]. Directly transmitting to high-dimensional images faces obstacles in terms of dimensionality and dynamic clarity. By embedding evolution in the gradient domain, the proposed method avoids these obstacles: The dynamic-adjustment and gradient-adaptive terms serve as spatially distributed controllers that modulate diffusion locally without an explicit global dynamic model. The PDE theory ensures the stability of curve evolution, and convergence comes from minimizing the energy functional.

This image-centric design maintains theoretical rigor while demonstrating unique value in real-world scenarios such as wildfire monitoring. The local adaptability of this model can robustly handle environmental uncertainties such as lighting changes and occlusion, providing reliable support for fire detection in drone patrols and emergency response. Future work will focus on model lightweighting to facilitate deployment in practical systems.

The dynamic system model for fire image processing is experimentally validated. Its gain depends on two adaptive terms: A dynamic adjustment term that balances denoising and edge preservation on pixels, and a gradient adaptation term that promotes evolution at weak edges and repairs classical active contour defects. Cross-dataset testing has shown stable advantages, but has revealed accuracy limits related to data complexity. The limitations lie in the fact that speed iteration optimization is not yet ultra real-time, and its robustness has not been tested in extreme weather conditions. Future work will reduce the burden on algorithms and make them more robust in harsher scenarios.5 Conclusion

A comprehensive image processing method based on dynamic models was proposed to address the insufficient edge detection accuracy, limited dynamic detection capability, and insufficient details in smoke images in traditional fire scene image processing systems. This study introduced nonlinear dynamic models and dynamic parameter adjustment mechanisms to efficiently suppress noise in fire scene images and achieve edge segmentation detection of flames and smoke. The proposed enhancement model improved the PSNR index by about 20% compared to median filtering on the RFSIE dataset and by about 25% on the NTIRE20 dataset. In terms of image segmentation, the accuracy on the FLAME dataset improved by 5.56% compared to FCN, and the IoU on the Fire Segmentation dataset improved by 9.09% compared with U-Net. In addition, in the classification task, the proposed model

improved the accuracy of flame classification by about 30.8% compared to median filtering, about 41.7% compared with Gaussian filtering, and about 21.4% compared with bilateral filtering. In terms of smoke classification, they increased by about 16.1%, 20%, and 9.1% respectively. In the background classification, there were improvements of approximately 8.6%, 8.6%, and 5.6%, respectively. In the flame category classification of image segmentation, the accuracy improved by about 4.8% compared to the U-Net model. Overall, the research has shown excellent results in improving the clarity and segmentation accuracy of fire scene image processing. However, the real-time performance and the ability to handle extreme weather fires still need improvement. Future research will optimize the computational efficiency and combine multi-source data to enhance the robustness to better adapt to diverse fire scenarios.

Funding

The research is supported by Jiangsu University Natural Science Foundation Project(21KJB510020), "Research on video intelligent processing and protection based on saliency region and deep learning method".

References

[1] Liu W, Shen Z, Xu S. CF-YOLO: a capable forest fire identification algorithm founded on YOLOv7 improvement. Signal, Image and Video Processing, 2024, 18(8): 6007-6017. https://doi.org/10.1007/s11760-024-03288-w

[2] Wu S, Sheng B, Fu G, Zhang D, Jian Y. Multiscale fire image detection method based on CNN and Transformer. Multimedia Tools and Applications, 2024, 83(16): 49787-49811. https://doi.org/10.1007/s11042-023-17482-4

[3] Oghabi E, Moghaddam R K, Kobravi H. A new strategy for fire detection based on analyzing the irregularity pattern of image contour. Signal, Image and Video Processing, 2024, 18(8): 6143-6155. https://doi.org/10.1007/s11760-024-03303-0

[4] Kwak D-K, Ryu J-K. A Study on Fire Detection Using Deep Learning and Image Filtering Based on Characteristics of Flame and Smoke. Journal of Electrical Engineering & Technology, 2023, 18(5): 3887-3895. https://doi.org/10.1007/s42835-023-01469-0

[5] Cao X, Wu J, Chen J, Li Z. Complex Scenes Fire Object Detection Based on Feature Fusion and Channel Attention. Arabian Journal for Science and Engineering, 2025, 50(10): 7587-7601. https://doi.org/10.1007/s13369-024-09471-y

[6] Yan F, Venegas-Andraca S E, Hirota K. Toward implementing efficient image processing algorithms on quantum computers. Soft Computing, 2023, 27(18): 13115-13127. https://doi.org/10.1007/s00500-021-06669-2

[7] Daglish J, Blacker A J, de Boer G, Crampton A, Hose D R J, Parsons A R, Kapur N. Determining Phase Separation Dynamics with an Automated Image Processing Algorithm. Org. Process Res. Dev., 2023, 27(4): 627-639. https://doi.org/10.1021/acs.oprd.2c00357

[8] Subarnan G M, Damodaran M, Madhu K, Rethinam G. Optimization of Image Processing Based MPPT Algorithm Using FSO Algorithm. Electric Power Components and Systems, 2023, 52(3): 364-380. https://doi.org/10.1080/15325008.2023.2220336

[9] Wang Z, Zhang T, Huang X. Explainable deep learning for image-driven fire calorimetry. Applied Intelligence, 2024, 54(1): 1047-1062. https://doi.org/10.1007/s10489-023-05231-x

[10] de Venâncio P V A B, Campos R J, Rezende T M, Lisboa A C, Barbosa A V. A hybrid method for fire detection based on spatial and temporal patterns. Neural Computing and Applications, 2023, 35(13): 9349-9361. https://doi.org/10.1007/s00521-023-08260-2

[11] Bhat, Younis Ahmad, Sheikh, Neyaz A. Windowed Octonionic Fourier Transform. Circuits, Systems, and Signal Processing, 2023, 42(5): 2872-2896. https://doi.org/10.1007/s00034-022-02241-x

[12] Nicola F, Tilli P. The Faber-Krahn inequality for the short-time Fourier transform. Inventiones mathematicae, 2022, 230(1): 1-30. https://doi.org/10.1007/s00222-022-01119-8

[13] Márquez A del P, Garrido T M, Recio E, de la Rosa R. Lie symmetries and exact solutions for a fourth-order nonlinear diffusion equation. Mathematical Methods in the Applied Sciences, 2022, 45(17): 10614-10627. https://doi.org/10.1002/mma.8387

[14] Dien N M, Nane E, Minh N D, Trong D D. Global solutions of nonlinear fractional diffusion equations with time-singular sources and perturbed orders. Fractional Calculus and Applied Analysis, 2022, 25(3): 1166-1198. https://doi.org/10.1007/s13540-022-00056-w

[15] Chernov A V. On the Exact Global Controllability of a Semilinear Evolution Equation. Differential Equations, 2024, 60(3): 374-392. https://doi.org/10.1134/S0012266124030091

[16] Girshick R, Donahue J, Darrell T, Malik J. Region-based convolutional networks for accurate object detection and segmentation. IEEE Transactions on Pattern Analysis and Machine Intelligence, 2016, 38(1): 142-158. https://doi.org/10.1109/TPAMI.2015.2437384

[17] Jebur R S, Zabil M H B M, Hammood D A, Cheng L K. A comprehensive review of image denoising in deep learning. Multimedia Tools and Applications, 2024, 83(20): 58181-58199. https://doi.org/10.1007/s11042-023-17468-2

[18] Xie W, Shao W, Li D, Li Y, Fang L. MIFNet: Multi-Scale Interaction Fusion Network for Remote Sensing Image Change Detection. IEEE Transactions on Circuits and Systems for Video Technology, 2025, 35(3): 2725-2739.

https://doi.org/10.1109/TCSVT.2024.3494820
[19] F. Zouari, K. B. Saad, and M. Benrejeb, "Adaptive backstepping control for a class of uncertain single input single output nonlinear systems," in 2013 10th International Multi-Conference on Systems, Signals & Devices (SSD), 2013, pp. 1-6. https://doi.org/10.1109/SSD.2013.6564134
[20] G. Rigatos, M. Abbaszadeh, B. Sari, P. Siano, G. Cuccurullo, and F. Zouari, "Nonlinear optimal control for a gas compressor driven by an induction motor," Results in Control and Optimization, vol. 11, p. 100226, 2023. https://doi.org/10.1016/j.rico.2023.100226
[21] A. Boulkroune, F. Zouari, and A. Boubellouta, "Adaptive fuzzy control for practical fixed-time synchronization of fractional-order chaotic systems," Journal of Vibration and Control, p. 10775463251320258, 2025. https://doi.org/10.1177/10775463251320258
[22] F. Zouari, K. B. Saad, and M. Benrejeb, "Robust neural adaptive control for a class of uncertain nonlinear complex dynamical multivariable systems," International Review on Modelling and Simulations, vol. 5, no. 5, pp. 2075-2103, 2012.
[23] L. Merazka, F. Zouari, and A. Boulkroune, "High-gain observer-based adaptive fuzzy control for a class of multivariable nonlinear systems," in 2017 6th International Conference on Systems and Control (ICSC), 2017, pp. 96-102. https://doi.org/10.1109/ICoSC.2017.7958728
[24] A. Boulkroune, S. Hamel, F. Zouari, A. Boukabou, and A. Ibeas, "Output-feedback controller based projective lag-synchronization of uncertain chaotic systems in the presence of input nonlinearities," Mathematical Problems in Engineering, vol. 2017, Article ID 8045803, 2017. https://doi.org/10.1155/2017/8045803